

Performance Analysis of OAMP Detection for ODDM Modulation in Satellite Communications

Yu Liu, Cunhua Pan, Tantaog Gong, Yinlu Wang, Ming Chen

Abstract—Towards future 6G wireless networks, low earth orbit (LEO) satellites have been widely considered as a promising component to enhance the terrestrial communications. To ensure the link reliability of high-mobility satellite communication scenarios, the emerging orthogonal delay-Doppler division multiplexing (ODDM) modulation has attracted significant research attention. In this paper, we study the diversity gain achieved by ODDM modulation along with the mathematical analysis and numerical simulations. Additionally, we propose an orthogonal approximate message passing (OAMP) algorithm based detector to harvest the diversity gain promised by ODDM modulation. By operating the linear and non-linear estimator iteratively, the orthogonal approximate message passing (OAMP) detector can utilize the sparsity of the effective delay-Doppler (DD) domain channel and extract the full diversity. Simulation results reveal the relationship between diversity gain and system parameters, and demonstrate that our proposed detector can achieve better performance than the conventional message passing methods with significantly reduced complexity.

Index Terms—ODDM, OAMP, satellite communications, diversity analysis

I. INTRODUCTION

In order to achieve the goal of global seamless communications, the low-earth-orbit (LEO) satellite communication is incorporated for the next generation mobile network. However, the high mobility of LEO satellites brings the severe Doppler effects, which is undoubtedly harmful to communication reliability. Recently, a series of delay-Doppler (DD) domain modulation has attracted significant research attention, which aims to convert the doubly-selective channel in the time-frequency (TF) domain into the almost non-fading channel in the DD domain. As a representative work in the DD domain modulation, the authors of [1] proposed the inverse symplectic finite Fourier transform (ISFFT) based orthogonal time frequency space (OTFS) modulation. However, this ISFFT-spread OTFS scheme employs TF domain orthogonal pulses that do not match the DD domain resolution, resulting in complicated input-output relation and performance degradation [2]. Henceforth, the authors of [3] proposed orthogonal delay-Doppler division multiplexing (ODDM) modulation as a promising and practical DD domain multi-carrier modulation. Since orthogonal pulses match DD domain resolutions,

ODDM is promising to have a simple input-output relation and practical implementation. Towards this end, an advanced detector design and corresponding performance analysis is essential to fulfill the potential of ODDM modulation.

Due to the similarity between ODDM modulation and OTFS modulation, several model-driven detectors of OTFS modulation can be applied to ODDM modulation, including maximum ratio combining detectors [4], variational Bayes based detectors [5], message passing (MP) based detectors [6] and their extended variations. Among the above mentioned detectors, orthogonal approximate message passing (OAMP) based detectors is promising due to their superior performance and reduced complexity. As the variation of the MP algorithm, the OAMP algorithm shows the potential to extract the full diversity of ODDM modulation. The proper approximations employed in the iterations reduce the computational complexity that is challenging for the conventional MP algorithm. Moreover, the denoiser of OAMP is divergence-free so that Onsager term vanishes and the de-correlated matrix is applied to ensure the orthogonality of the input and output errors, beneficial to extend the scope to more general unitarily-invariant channel matrices and guarantee detection reliability [7].

Among the existing research concerning ODDM modulation, the theoretical error performance has not been extensively studied as that of OTFS modulation yet. We note that the authors of [3] suggested that ODDM can achieve full time-frequency diversity. However, this suggestion has not been established through analysis or simulations. To fill this gap in this work, we aim to investigate the diversity gain of ODDM with maximum likelihood (ML) detection and the corresponding error performance under the OAMP detection algorithm. The key findings and contributions in this work can be summarized as follows:

- 1) We derive the unconditional performance bound of ODDM with ML detection by leveraging the conditional pairwise error probability. Furthermore, the diversity order of ODDM is obtained by computing the minimum rank of the potential difference matrices. These theoretical results provide essential analytical insights for our simulations.
- 2) Additionally, we design an OAMP-based detector for ODDM and evaluate the BER performance of the proposed detector by numerical simulations. The simulated performance follows the trends of theoretical bounds and indicates that the proposed OAMP detector can achieve better performance with reduced complexity. Moreover, the simulations demonstrate that ODDM achieves simi-

(Corresponding author: Ming Chen.)

Yu Liu, Cunhua Pan, Tantaog Gong, Ming Chen are with are with the National Mobile Communications Research Laboratory, Southeast University, Nanjing, 210096, China (e-mail: {liuyu_1994, cpan, gongtantaog, chenming}@seu.edu.cn).

Yinlu Wang is with the School of Communication and Information Engineering, Nanjing University of Posts and Telecommunications, Nanjing, 210003, China (e-mail: yinluwang@njupt.edu.cn).

lar comparable BER performance to OTFS with significantly lower out-of-band emissions (OOBE).

II. SYSTEM MODEL

In this paper, we consider a point-to-point LEO satellite communication system that employs ODDM. Without loss of generality, let us consider ODDM transmitter as follows. Let M be the number of delay bins/subcarriers and N be the number of Doppler bins/time slots, respectively. In the term of time-frequency domain, the corresponding subcarrier spacing and time slot duration are respectively given by Δf and T , which obey $\Delta f = \frac{1}{T}$. In the term of delay-Doppler domain, the delay resolution of the signal is $\frac{1}{M\Delta f}$, and the Doppler resolution of the signal is $\frac{1}{NT}$. Let $\mathbf{X} \in \mathbb{A}^{M \times N}$ be the transmitted symbol matrix in the DD domain. To be specific, let $x[m, n]$ represent the (m, n) -th element in \mathbf{X} , and $\mathbf{x} \in \mathbb{A}^{MN \times 1}$ be the vectorization of \mathbf{X} . According to [3], ODDM is a multicarrier (MC) modulation, which aims to modulate DD domain symbols into M staggered MC symbols, with symbol period of NT , subcarrier spacing of $\frac{1}{NT}$ and symbol interval of $\frac{T}{M}$, respectively. Then the CP-free waveform of the DD plane MC modulation is given by

$$s(t) = \sum_{m=0}^{M-1} \sum_{n=0}^{N-1} x[m, n] \hat{g}_{\text{tx}} \left(t - m \frac{T}{M} \right) e^{j2\pi \frac{n}{NT} (t - m \frac{T}{M})}, \quad (1)$$

where $\hat{g}_{\text{tx}}(t)$ is the transmit pulse. Note that $\hat{g}_{\text{tx}}(t)$ is a DD domain orthogonal pulse with respect to the DD plane resolutions. It can be obtained by $\hat{g}_{\text{tx}}(t) = \sum_{\hat{n}=0}^{N-1} a(t - \hat{n}T)$, where $a(t)$ denotes a time-symmetric real-valued square-root Nyquist pulse that spans a time duration of $2Q\frac{T}{M}$, with Q being an integer and $2Q \ll M$. The pulse satisfies $a(t) = 0$ for $t \notin (-Q\frac{T}{M}, Q\frac{T}{M})$. Without loss of generality, suppose that $\int_{-\infty}^{+\infty} |a(t)|^2 dt = \frac{1}{N}$, thus $\int_{-\infty}^{+\infty} |\hat{g}_{\text{tx}}(t)|^2 dt = 1$. Finally, considering the cyclic prefix (CP), we extend the definition of \hat{g}_{tx} to $u_{\text{cp}}(t) = \sum_{\hat{n}=-1}^{N-1} a(t - \hat{n}T)$. Without loss of generality, we assume that the maximum delay and Doppler shift of the channel are $(L-1)\frac{T}{M}$ and $K\frac{1}{NT}$, respectively. Then, the CP-included ODDM waveform spanning over $-(L+Q-1)\frac{T}{M} \leq t \leq NT + (Q-1)\frac{T}{M}$ becomes

$$s_{\text{cp}}(t) = \sum_{m=0}^{M-1} \sum_{n=0}^{N-1} x[m, n] u_{\text{cp}} \left(t - m \frac{T}{M} \right) e^{j2\pi \frac{n}{NT} (t - m \frac{T}{M})}, \quad (2)$$

where $u_{\text{cp}}(t) = u(t)$ for $t \in (-Q\frac{T}{M}, (N-1)T + Q\frac{T}{M})$ and $u_{\text{cp}}(t) = 0$ for $t \in (-T + Q\frac{T}{M}, -Q\frac{T}{M})$.

At the receiver side, the received ODDM signals for $-(L+Q-1)\frac{T}{M} \leq t \leq NT + (L+Q-2)\frac{T}{M}$ can be expressed as

$$\begin{aligned} y(t) &= \sum_{p=1}^P h_p s_{\text{cp}}(t - \tau_p) e^{j2\pi \nu_p (t - \tau_p)} + z(t) \\ &= \sum_{p=1}^P \sum_{m=0}^{M-1} \sum_{n=0}^{N-1} h_p x[m, n] u_{\text{cp}} \left(t - (m + l_p) \frac{T}{M} \right) \\ &\quad \cdot e^{j2\pi \frac{n+k_p}{NT} (t - (m+l_p) \frac{T}{M})} e^{j2\pi \frac{k_p m}{MN}} + z(t), \end{aligned} \quad (3)$$

where P is the number of multipaths and h_p refers to the channel gain of the p -th path. Note that, $l_p = \frac{\tau_p}{M\Delta f}$ denotes

the delay index, and τ_p is the delay shift of the p -th path. $k_p = \frac{\nu_p}{NT}$ depicts Doppler index, and ν_p represents Doppler shift of the p -th path. $z(t)$ indicates the noise in the DD domain. Passing the matched filter, the received ODDM signal in the DD domain is obtained as (4), where $z[m, n]$ indicates the DD domain noise sample.

The symbol-wise input-output relation can be transformed into a vectorized form,

$$\mathbf{y} = \mathbf{H}\mathbf{x} + \mathbf{z}, \quad (5)$$

where $\mathbf{y} \in \mathbb{C}^{MN \times 1}$ and $\mathbf{z} \in \mathbb{C}^{MN \times 1}$ stand for the vectorized form of the received signal and noise in the DD domain. $\mathbf{H} \in \mathbb{C}^{MN \times MN}$ is the effective channel matrix, given by

$$\mathbf{H} = \begin{bmatrix} \mathbf{H}_0^0 & & \mathbf{H}_0^{L-1} \mathbf{D} & \cdots & \mathbf{H}_1^0 \mathbf{D} \\ \vdots & \ddots & & & \vdots \\ \mathbf{H}_{L-1}^{L-1} & \cdots & \mathbf{H}_0^{L-1} & \mathbf{0} & \mathbf{H}_{L-1}^{L-2} \mathbf{D} \\ & \ddots & \ddots & \ddots & \ddots \\ \mathbf{0} & \mathbf{H}_{L-1}^{M-1} & \cdots & \cdots & \mathbf{H}_0^{M-1} \end{bmatrix}, \quad (6)$$

where $\mathbf{H}_l^m = \sum_{\hat{k}=-K}^K g(\hat{k} + K + 1, l) e^{j2\pi \frac{\hat{k}(m-l)}{MN}} \mathbf{C}^{\hat{k}}$ denotes the sub-channel block and $\mathbf{D} = \text{diag}\{1, e^{-j\frac{2\pi}{N}}, \dots, e^{-j\frac{2\pi(N-1)}{N}}\}$ denotes the additional phase rotation. Note that in \mathbf{H}_l^m , \mathbf{C} is the $N \times N$ cyclic permutation matrix and $g(\cdot)$ is given by

$$g(\hat{k} + K + 1, l) = \begin{cases} h_p, & \text{if } \hat{k} + K + 1 = k_p, l = l_p, \\ 0, & \text{Otherwise.} \end{cases} \quad (7)$$

Apparently, \mathbf{H} is a sparse matrix.

III. OAMP BASED DETECTOR FOR ODDM

In this section, we briefly introduce OAMP and explore its application to ODDM detection.

A. OAMP detector

The OMAP algorithm is designed to solve the sparse linear inverse problem like (5), and it refers to the following recursion:

$$\text{LE: } \mathbf{r}_t = \mathbf{x}_t + \mathbf{W}_t (\mathbf{y} - \mathbf{H}\mathbf{x}_t) \quad (8a)$$

$$\text{NLE: } \mathbf{x}_{t+1} = \eta_t(\mathbf{r}_t), \quad (8b)$$

where η_t is a component-wise Lipschitz continuous function of \mathbf{r}_t . This OAMP based detector is decomposed into the iteration of a ‘divergence-free’ linear estimator (LE) and a ‘divergence-free’ non-linear estimator (NLE) [8]. The LE aims to eliminate the effects of multipath interference, then the NLE is designed to reduce the Gaussian noise and improve the quality of estimation. Through operating the two estimators iteratively, the posterior probability $P(\mathbf{x}|\mathbf{y}, \mathbf{H})$ can be decoupled into a series of $P(x_i|\mathbf{y}, \mathbf{H})$.

As shown in (8), the main idea of OMAP is to design a linear transformer \mathbf{W}_t and a denoiser $\eta_t(\cdot)$ satisfying orthogonality and divergence-free. For convenience, we define the input-output errors as $\mathbf{q}_t = \hat{\mathbf{x}} - \mathbf{x}$ and $\mathbf{p}_t = \mathbf{r}_t - \mathbf{x}$, where

$$y[m, n] = \begin{cases} \sum_{p=1}^P h_p x [m - l_p, [n - k_p]_N] e^{j2\pi \frac{k_p(l-l_p)}{MN}} + z[m, n], & m - l_p \geq 0 \\ \sum_{p=1}^P h_p e^{-j2\pi \frac{(n-k_p)N}{N}} x [[m - l_p]_M, [n - k_p]_N] e^{j2\pi \frac{k_p(l-l_p)}{MN}} + z[m, n], & m - l_p < 0 \end{cases} \quad (4)$$

$\hat{\mathbf{x}}_t$ is the estimation of \mathbf{x} at the t -th iteration. Also, we define the error variance of the LE and NLE as

$$\nu_t^2 = \frac{1}{MN} \mathbb{E}\{\|\mathbf{q}_t\|_2^2\}, \quad \tau_t^2 = \frac{1}{MN} \mathbb{E}\{\|\mathbf{p}_t\|_2^2\}. \quad (9)$$

Furthermore, the structure of \mathbf{W}_t is derived from the LMMSE decorrelated matrix, which implies

$$\mathbf{W}_t = \frac{MN}{\text{Tr}(\hat{\mathbf{W}}_t \mathbf{H})} \hat{\mathbf{W}}_t, \quad (10)$$

where $\hat{\mathbf{W}}_t = \mathbf{H}^T (\mathbf{H}\mathbf{H}^T + \frac{\sigma^2}{\nu_t^2} \mathbf{I})^{-1}$. This linear estimator aims to decouple the linear mixing model (5) into MN parallel models, i.e., $r_t = x + w_t$.

Henceforth, the principles of the OAMP based detector for ODDM can be summarized in Algorithm 1, where $\mathbf{B}_t = \mathbf{I} - \mathbf{W}_t \mathbf{H}$.

Algorithm 1 OAMP based detector for ODDM

Input: \mathbf{y}, \mathbf{H} , the maximum number of iterations T

Output: $\hat{\mathbf{x}}$

Initialization: $\hat{\mathbf{x}}_0 = \mathbf{0}, \nu_0^2 = 1$

- 1: **while** $t \leq T$ **do**
 - 2: $\mathbf{r}_t = \hat{\mathbf{x}}_t + \mathbf{W}_t (\mathbf{y} - \mathbf{H}\hat{\mathbf{x}}_t)$
 - 3: $\tau_t^2 = \frac{1}{2MN} \text{Tr}(\mathbf{B}_t \mathbf{B}_t^H) \nu_t^2 + \frac{1}{4MN} \text{Tr}(\mathbf{W}_t \mathbf{W}_t^H) \sigma^2$
 - 4: $\hat{\mathbf{x}}_{t+1} = \mathbb{E}\{\mathbf{x} | \mathbf{r}_t, \tau_t\}$
 - 5: $\nu_{t+1}^2 = \frac{\|\mathbf{y} - \mathbf{H}\hat{\mathbf{x}}_{t+1}\|_2^2 - MN\sigma^2}{\text{Tr}(\mathbf{H}^H \mathbf{H})}$
 - 6: **end while**
-

Furthermore, the denoiser is given by

$$\mathbb{E}\{\mathbf{x} | \mathbf{r}_t, \tau_t\} = \frac{\sum_{x_i \in \mathbb{A}} x_i e^{-\frac{\|r_i - x_i\|_2^2}{\tau_t^2}}}{\sum_{x_i \in \mathbb{A}} e^{-\frac{\|r_i - x_i\|_2^2}{\tau_t^2}}}. \quad (11)$$

The Bayesian MMSE estimator and the posterior mean estimator in Algorithm 1 are orthogonal if the channel matrix is unitary invariant. By applying the element-wise estimation to the decoupled signal, the OAMP algorithm is Bayes optimal.

IV. DIVERSITY ANALYSIS OF ODDM

In this section, in order to study the diversity of ODDM, we consider an alternative formulation of input-output relation of this ODDM scheme given by

$$\mathbf{y} = \Phi(\mathbf{x})\mathbf{h} + \mathbf{z}, \quad (12)$$

where $\mathbf{h} = [h_1, h_2, \dots, h_p]^T \in \mathbb{C}^{P \times 1}$ is the vector of complex channel gains, and the small-scale channel coefficient h_p follows $\mathcal{N}(0, 1/P)$. $\Phi(\mathbf{x}) \in \mathbb{C}^{MN \times P}$ is the concatenated matrix given by

$$\Phi(\mathbf{x}) = [\Xi_1 \mathbf{x} | \dots | \Xi_P \mathbf{x}], \quad (13)$$

and $\Xi_p \in \mathbb{C}^{MN \times MN}$ is defined in (29).

For convenience, we normalize the elements of \mathbf{x} , thus the energy allocated to each symbol is one. The transmitting signal-to-noise ratio (SNR), denoted by γ , is therefore given

by $\gamma = 1/N_0$. Assuming perfect channel estimation, the conditional pairwise error probability (PEP) of the transmitting symbols \mathbf{x} and the receiving symbols $\hat{\mathbf{x}}$ is given by [9],

$$P(\mathbf{x} \rightarrow \hat{\mathbf{x}} | \mathbf{h}, \mathbf{x}) = \mathcal{Q} \left(\sqrt{\frac{\|[\Phi(\mathbf{x}) - \Phi(\hat{\mathbf{x}})]\mathbf{h}\|_2^2}{2N_0}} \right), \quad (14)$$

where $\mathcal{Q}(\cdot)$ is the tail distribution function of the standard normal distribution. Henceforth, the expected PEP become

$$P(\mathbf{x} \rightarrow \hat{\mathbf{x}}) = \mathbb{E}_{\mathbf{h}} \left[\mathcal{Q} \left(\sqrt{\frac{\gamma \|[\Phi(\mathbf{x}) - \Phi(\hat{\mathbf{x}})]\mathbf{h}\|_2^2}{2}} \right) \right]. \quad (15)$$

Rewrite $\|[\Phi(\mathbf{x}) - \Phi(\hat{\mathbf{x}})]\mathbf{h}\|_2^2$ as

$$\|[\Phi(\mathbf{x}) - \Phi(\hat{\mathbf{x}})]\mathbf{h}\|_2^2 = \mathbf{h}^H [\Phi(\mathbf{x}) - \Phi(\hat{\mathbf{x}})]^H [\Phi(\mathbf{x}) - \Phi(\hat{\mathbf{x}})] \mathbf{h}. \quad (16)$$

The matrix $[\Phi(\mathbf{x}) - \Phi(\hat{\mathbf{x}})]^H [\Phi(\mathbf{x}) - \Phi(\hat{\mathbf{x}})]$ is Hermitian matrix that can be transformed into

$$[\Phi(\mathbf{x}) - \Phi(\hat{\mathbf{x}})]^H [\Phi(\mathbf{x}) - \Phi(\hat{\mathbf{x}})] = \mathbf{U} \mathbf{\Lambda} \mathbf{U}^H, \quad (17)$$

where $\mathbf{U} \in \mathbb{C}$ is the unitary matrix and $\mathbf{\Lambda} = \text{diag}\{\lambda_1^2, \lambda_2^2, \dots, \lambda_P^2\}$ with λ_p being the p -th singular value of the difference matrix $\Delta(\mathbf{x}, \hat{\mathbf{x}}) = \Phi(\mathbf{x}) - \Phi(\hat{\mathbf{x}})$. Thus, (16) can be simplified as

$$\|[\Phi(\mathbf{x}) - \Phi(\hat{\mathbf{x}})]\mathbf{h}\|_2^2 = \tilde{\mathbf{h}} \mathbf{\Lambda} \tilde{\mathbf{h}}^H = \sum_{p=1}^r \lambda_p^2 |\tilde{h}_p|^2, \quad (18)$$

where r denotes the rank of the difference matrix $\Delta(\mathbf{x}, \hat{\mathbf{x}})$. Substituting (18) into (15), the expected PEP can become

$$P(\mathbf{x} \rightarrow \hat{\mathbf{x}}) = \mathbb{E}_{\mathbf{h}} \left[\mathcal{Q} \left(\sqrt{\frac{\gamma \sum_{p=1}^r \lambda_p^2 |\tilde{h}_p|^2}{2}} \right) \right]. \quad (19)$$

According to [9], the expected PEP can be simplified to get the following upper bound,

$$P(\mathbf{x} \rightarrow \hat{\mathbf{x}}) \leq \prod_{p=1}^r \frac{1}{1 + \frac{\gamma \lambda_p^2}{4P}}. \quad (20)$$

In the case of Rayleigh fading, (20) can be further simplified as

$$P(\mathbf{x} \rightarrow \hat{\mathbf{x}}) \leq \frac{1}{\prod_{p=1}^r \lambda_p^2 / P} \left(\frac{\gamma}{4} \right)^{-r}. \quad (21)$$

Henceforth, the upper bound on the average bit error probability (BEP) P_e can be expressed as

$$P_e \leq \frac{1}{Q^{MN}} \sum_{\mathbf{x} \in \mathbb{A}^{MN}} \sum_{\hat{\mathbf{x}} \neq \mathbf{x}} \frac{d_b(\mathbf{x}, \hat{\mathbf{x}})}{MN \log_2 Q} \left(\prod_{p=1}^r \lambda_p^2 \right)^{-1} \left(\frac{\gamma}{4P} \right)^{-r}. \quad (22)$$

where Q is the modulation order and $d_b(\mathbf{x}, \hat{\mathbf{x}})$ is the difference in number of information bits between \mathbf{x} and $\hat{\mathbf{x}}$. From (20) and (21), it can be seen that the exponent of the SNR term γ is r , which illustrates that the rank of difference matrix $\Delta(\mathbf{x}, \hat{\mathbf{x}})$ dominates the PEP. Furthermore, the PEP with the minimum

value of r dominates the overall BEP as well. Finally, the diversity order of ODDM is defined as

$$\rho \triangleq \min_{\mathbf{x} \neq \hat{\mathbf{x}}} \text{rank}(\Delta(\mathbf{x}, \hat{\mathbf{x}})). \quad (23)$$

As indicated by (23), the diversity order is closely related to the minimum rank of the difference matrix $\Delta(\mathbf{x}, \hat{\mathbf{x}})$. This minimum rank is determined by the delay and Doppler shift, denoted as l_p and k_p . Consequently, the minimum potential diversity order for ODDM is one, while the maximum potential diversity order can reach P .

A. Lower Bound on the Average BER

In this subsection, we derive a lower bound on the BER of ODDM. This lower bound, along with the simulation results, can provide the insights into the trends of the BER performance with SNR increasing. According to [10], the lower bound on the BER can be obtained by summing the PEPs corresponding to all the pairs \mathbf{x} and $\hat{\mathbf{x}}$, whose difference matrix $\Delta(\mathbf{x}, \hat{\mathbf{x}})$ has the rank that equals to one. With this assumption, the lower bound on the BER is given by

$$\text{BER} \geq \frac{1}{Q^{MN}} \sum_{\text{rank}=1} P(\mathbf{x} \rightarrow \hat{\mathbf{x}}). \quad (24)$$

When $\Delta(\mathbf{x}, \hat{\mathbf{x}})$ has rank one, the only one non-zero singular value of the difference matrix equals to $\sqrt{4PMN}$. Therefore, the PEP with $\Delta(\mathbf{x}, \hat{\mathbf{x}})$ having rank one can be simplified to

$$P(\mathbf{x} \rightarrow \hat{\mathbf{x}}) = \mathbb{E} \left[\mathcal{Q} \left(\sqrt{2\gamma PMN |\tilde{h}_1|^2} \right) \right]. \quad (25)$$

Since $\tilde{h}_1 \sim \mathcal{CN}(0, 1/P)$, evaluating the expectation in (25) gives [9]

$$P(\mathbf{x} \rightarrow \hat{\mathbf{x}}) = \frac{1}{2} \left(1 - \sqrt{\frac{MN}{MN + \gamma^{-1}}} \right). \quad (26)$$

Therefore, the lower bound is obtained as

$$\text{BER} \geq \frac{\kappa}{Q^{MN}} \frac{1}{2} \left(1 - \sqrt{\frac{MN}{MN + \gamma^{-1}}} \right), \quad (27)$$

where κ denotes the number of difference matrices having rank one. At high SNRs, this expression can be further simplified to

$$\text{BER} \geq \frac{\kappa}{Q^{MN}} \frac{1}{4\gamma MN}. \quad (28)$$

Observes that (28) serves as the approximated diversity order lower bound on the average BER and its value depends on the ratio $\frac{\kappa}{Q^{MN}}$. As the values M and N increase, the Q^{MN} term dominates the ratio $\frac{\kappa}{Q^{MN}}$, hence increasing M and N can reduce the lower bound in (28).

V. SIMULATION RESULTS

A. Theoretical Performance Analysis

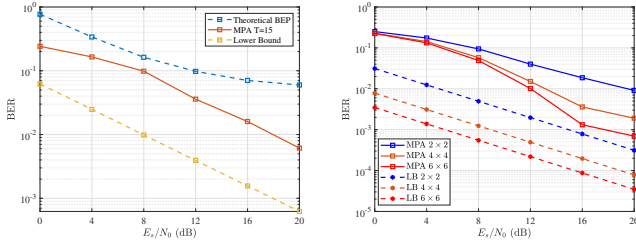
In this subsection, we perform the simulations under the simplified assumption to illustrate the upper and lower bound of the BER performance with the maximum likelihood detection. For ease of simulations, the system model is simplified

to $M = N = 2$, and the modulation order is set to 4QAM. The channel model is set according to (6), and the number of paths is set to $P = 4$. The path delay taps are chosen from $l_p \in \{0, \dots, M-1\}$, and the Doppler taps are chosen from $k_p \in \{0, \dots, N-1\}$. Especially, E_s is the energy allocated to each symbol, and E_s/N_0 illustrates the transmit signal-to-noise ratio (SNR). In addition to the simulated BER curve, in Fig. 1a, we also plot the BEP as the upper bound and the lower bound from (28) for the considered system. It is observed that the simulated BER performance lies between the lower bound and the upper bound. Although the bound is not tight, it can still provide the insights for us from the trends. It can be seen from the figure that the simulated BER shows a higher diversity order in the medium to high E_s/N_0 regime, before its slope changes to be close to that of the lower bound. Fig. 1b shows the BER performance and lower bound for three systems of different frame sizes $\{M, N\}$. It is observed that the BER curves in all three systems meet the diversity order one lower bound at the high SNR regime. Meanwhile, the BER curves with the larger frame sizes show a diversity order higher than one in the low to medium SNR regime before meeting the diversity order one. This means that the BER curves can decrease with a higher slope for larger $\{M, N\}$ before it changes the slope and meets the diversity order one lower bound of (28).

B. Practical Performance Comparison

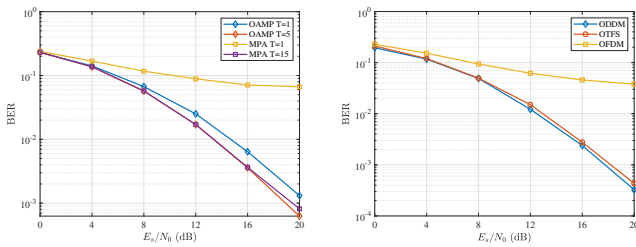
This subsection illustrates the BER performance of the OAMP detector for ODDM under the NTN-TDL channel model given by 3GPP [11]. The system with $M = 64, N = 16$ employs 4QAM symbol mapping. The carrier frequency of C band and the subcarrier spacing of 15 kHz are considered. The delay spread employs $\tau_s = 300$ ns and the Doppler spread employs $\nu_s = 3750$ Hz for channel generation. In Fig. 2a, we compare the BER performance of the OAMP-based detector and the ordinary MP detector with different iteration settings under the practical NTN-TDL-B model. We observe that with E_s/N_0 increasing, the BER performance of both detectors becomes better. It can be clearly observed that the OAMP-based detector performs better than the MP detector significantly when the number of iterations is low. With one iteration, our OAMP-based detector outperforms the MP detector by up to 20 dB in the high SNR regime. Moreover, the MP detector needs three times more iterations to achieve the performance close to that of the OAMP-based detector. This phenomenon illustrates the superior efficiency of the OAMP-based detector, which benefits from its enhanced exploitation of the sparsity in the effective DD domain channel. Additionally, in Fig. 2b, we conduct a comparison of the BER performance of various modulation methods under the NTN-TDL-B model. In this comparison, ODDM and OTFS modulation both utilize OAMP detector with 10 iterations, while OFDM modulation employs 1tap method proposed in [6]. The simulations show that both OTFS and ODDM modulation outperform OFDM modulation, indicating the advantages of DD domain modulation. Moreover, the BER performance of both two DD domain modulation methods is found to be quite similar.

$$\mathbb{E}_p[\cdot, q] = \begin{cases} e^{j2\pi \frac{k_p(m-l_p)}{MN}}, & \text{if } m \geq l_p \text{ and } q = [m - l_p]_M + M[n - k_p]_N \\ e^{j2\pi \frac{k_p(m-l_p)}{MN}} e^{-j2\pi \frac{[n-k_p]_N}{N}}, & \text{if } m < l_p \text{ and } q = [m - l_p]_M + M[n - k_p]_N \\ 0, & \text{otherwise} \end{cases} \quad (29)$$



(a) Upper bound, lower bound, and the simulated BER performance. (b) BER performance and lower bound for different frame sizes.

Fig. 1: The theoretical and simulated performance of ODDM versus E_b/N_0 .



(a) The BER performance of ODDM with various detection methods. (b) The BER performance of various modulation methods.

Fig. 2: The BER performance versus E_b/N_0 under NTN-TDL-B model.

Meanwhile, we examine the power spectral density (PSD) of transmitted DD communication signals in Fig. 3. Because of the square-root Nyquist pulses based shaping, ODDM exhibits significant OOB reduction comparing to OTFS, achieving an improvement of up to 30 dB at the band edges. Due to the severe OOB, the bandwidth of a fully-loaded OTFS system based on the TF domain OFDM interpretation is not well-defined. In the practice, OTFS systems can not fully utilize all subchannels as some null subcarriers placed at the band edges to sharpen the spectrum, leading to the reduced spectral efficiency. Furthermore, because the information-carrying symbols are modulated in the DD domain, it is still unclear how to arrange them such that the edge subcarriers in the TF domain remain unloaded after the ISFFT. On the other hand, ODDM systems can fully utilize the subchannels. By adjusting the roll-off factor, a trade-off between the excess bandwidth and OOB can be struck to achieve the desirable spectral efficiency. This observation verifies the practical advantage of ODDM.

VI. CONCLUSION

In this paper, we investigated the correlation of the diversity gain and parameters of the system and channel for ODDM modulation. We revealed that the minimum diversity gain order of the ML detection for ODDM modulation is the number of resolvable paths, henceforth the minimum diversity gain order can be one. Moreover, the analysis showed that increasing

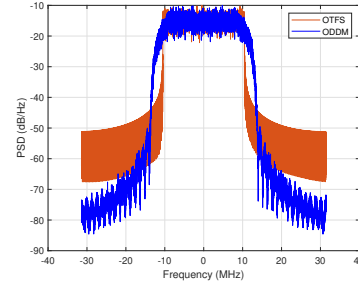


Fig. 3: PSD comparison, $M = 512$, $N = 32$, 16-QAM.

the frame size can improve the BER performance even if the specific diversity gain order had taken over the regime. Further, we proposed a OAMP based detector for ODDM transmission with the reduced complexity comparing to the conventional MP algorithm. The simulation results illustrated that our proposed detector can achieve superior performance with fewer iteration numbers than the conventional MP algorithm. Besides, the numerical simulations validated our analysis of the diversity gain. In addition, we compared the performance of ODDM with other modulation schemes. The simulation results demonstrated that ODDM achieved comparable performance to OTFS with the significantly reduced OOB.

REFERENCES

- [1] R. Hadani, S. Rakib, M. Tsatsanis, A. Monk, A. J. Goldsmith, A. F. Molisch, and R. Calderbank, "Orthogonal time frequency space modulation," in *2017 IEEE Wireless Communications and Networking Conference (WCNC)*, 2017, pp. 1–6.
- [2] S. Gopalam, I. B. Collings, S. V. Hanly, H. Inaltekin, S. R. B. Pillai, and P. Whiting, "Zak-otfs implementation via time and frequency windowing," *IEEE Transactions on Communications*, vol. 72, no. 7, pp. 3873–3889, 2024.
- [3] H. Lin and J. Yuan, "Orthogonal delay-doppler division multiplexing modulation," *IEEE Transactions on Wireless Communications*, vol. 21, no. 12, pp. 11 024–11 037, 2022.
- [4] T. Thaj and E. Viterbo, "Low complexity iterative rake decision feedback equalizer for zero-padded otfs systems," *IEEE Transactions on Vehicular Technology*, vol. 69, no. 12, pp. 15 606–15 622, 2020.
- [5] W. Yuan, Z. Wei, J. Yuan, and D. W. K. Ng, "A simple variational bayes detector for orthogonal time frequency space (otfs) modulation," *IEEE Transactions on Vehicular Technology*, vol. 69, no. 7, pp. 7976–7980, 2020.
- [6] P. Raviteja, K. T. Phan, Y. Hong, and E. Viterbo, "Interference cancellation and iterative detection for orthogonal time frequency space modulation," *IEEE Transactions on Wireless Communications*, vol. 17, no. 10, pp. 6501–6515, 2018.
- [7] Q. Zou and H. Yang, "A concise tutorial on approximate message passing," 2022. [Online]. Available: <https://arxiv.org/abs/2201.07487>
- [8] J. Ma and L. Ping, "Orthogonal amp," *IEEE Access*, vol. 5, pp. 2020–2033, 2017.
- [9] D. Tse and P. Viswanath, *Fundamentals of wireless communication*. USA: Cambridge University Press, 2005.
- [10] G. D. Surabhi, R. M. Augustine, and A. Chockalingam, "On the diversity of uncoded otfs modulation in doubly-dispersive channels," *IEEE Transactions on Wireless Communications*, vol. 18, no. 6, pp. 3049–3063, 2019.
- [11] 3rd Generation Partnership Project (3GPP), "3GPP TR 38.811: Study on New Radio (NR) to support non-terrestrial networks," 3GPP, Technical Report TR 38.811, 2020.